Proceedings of the Institution of Civil Engineers
Structures & Buildings 160
Month 2007 Issue SB1
Pages 1–16
doi: 10.1680/stbu.2007.160.1.1

Paper 07–00020R1
Received 31/05/2007
Accepted 20/09/2007

Keywords: shells

J. A. O. Barros
Associate Professor of Civil Engineering, University of Minho, Portugal

P. B. Lourenço
Professor of Civil Engineering, University of Minho, Portugal

J. T. Oliveira
Postdoctoral collaborator, University of Minho, Portugal

E. Bonaldo
PhD student, University of Minho, Portugal

ice
Institution of Civil Engineers

Experimental characterisation of a new reinforced brick masonry shell system

J. A. O. Barros, P. B. Lourenço, J. T. Oliveira and E. Bonaldo

The main aim of the current paper is to describe the experimental research carried out at the University of Minho regarding the development of an innovative reinforced brick masonry shell structural system. The concept of the system is based on the work of the engineer Eladio Dieste, and focuses on the prefabrication industry. The structural system is composed of a layer of clay bricks, reinforced concrete joints and a reinforced concrete cover layer. The constituent materials of the structural system were selected according to the necessary requirements in terms of mechanical properties and pre-fabrication technology. To analyse the interaction between the intervening materials, flexural, shear and biaxial tests with representative panels were carried out. To validate the developed structural system, a full scale shell was built and tested under monotonic vertical load applied at a quarter of its span. The shell performance revealed that the developed structural system is suitable for the proposed application.

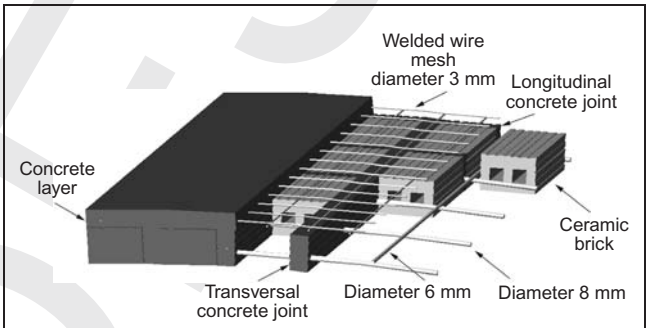

Fig. 1. Developed structural system

1. INTRODUCTION

Taking into account the intrinsic advantages of clay bricks, Eladio Dieste,[1,2] a Uruguayan engineer, built impressive reinforced masonry shells. Dieste's shells were composed of clay bricks, steel reinforced joints and a topping made of mortar. This type of shells used a low-cost technology and was aesthetically appealing and structurally efficient. The most well-known example of the Dieste system is the double curvature and free-standing vaults, built mainly in South America.

From the economic point-of-view, the Dieste system should be based on pre-fabrication technology in order to become a competitive building system for industrialised countries. This is the aim of the ISO-BRICK European project (2002–2004), in which the research shown in the present work was integrated. The developed structural system is illustrated in Fig. 1, including hollow clay bricks arranged in a non-interlocking (or stacked) pattern, reinforced longitudinal and transversal joints using micro-concrete and a reinforced concrete layer on the top of the shell. A comprehensive experimental programme was carried out, see Fig. 2, to select the materials adopted in the structural system and to characterise their properties, as well as tests at the structural level. As Fig. 2(b) shows, the tests carried out for the material characterisation include: tension and compression tests with brick specimens; tension, compression and bending with concrete specimens; tension tests with coupons of steel bars; and bond tests with masonry specimens.

In general, shell structures have membrane force components, bending moment components and out-of-plane shear force components (see Fig. 2). To assess the performance of the structural system submitted to in-plane shear (with distinct levels of lateral confinement), triplet shear tests with panel prototypes were carried out, see Fig. 2(c1). Double curvature shells are submitted to biaxial compression and, to evaluate the behaviour of the structural system submitted to biaxial compression loading configurations of distinct axial ratio, see Fig. 2(c2), the servo biaxial test system shown in Fig. 3 was built. A shell structure is submitted to positive and negative bending moments owing to, for example, seismic loading (here positive bending moments are assumed to apply tension in the lower part of the system). To assess the performance of the developed system when subjected to bending, four line load bending test series were carried out with representative panels, see Fig. 2(c3). Shear failures can occur near the shell supports or concentrated loads. To assess the out-of-plane shear resistance of the developed structural system, panel

Article number = 700020

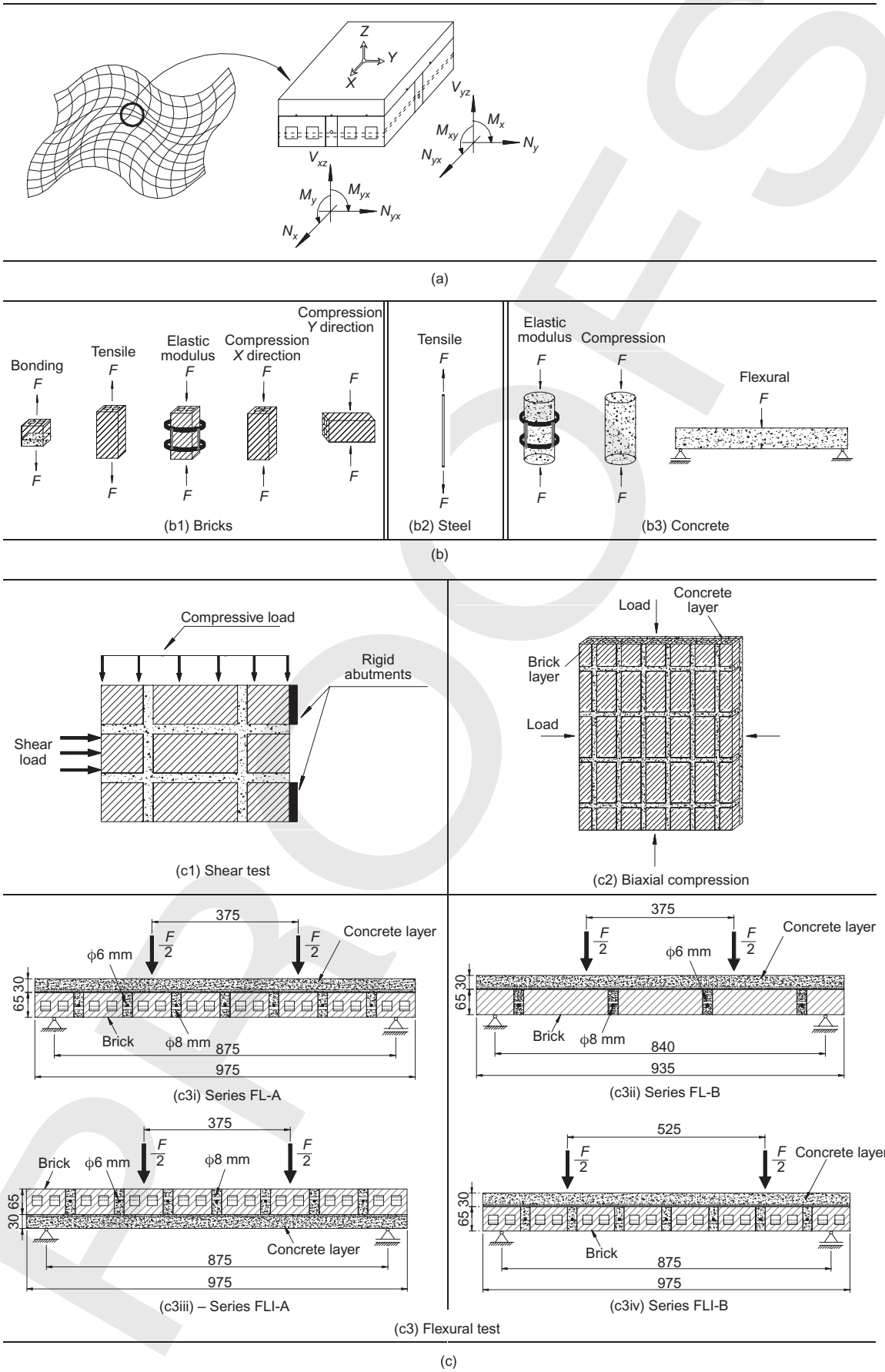

Fig. 2. Experimental programme: (a) shell force components; (b) material tests; (c)structural tests

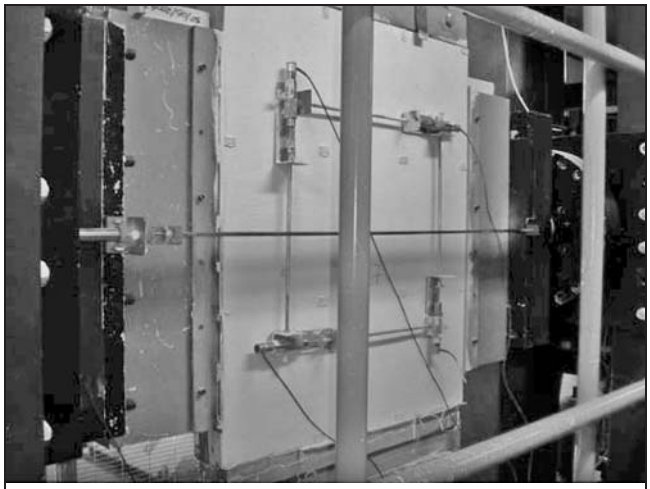

(a)

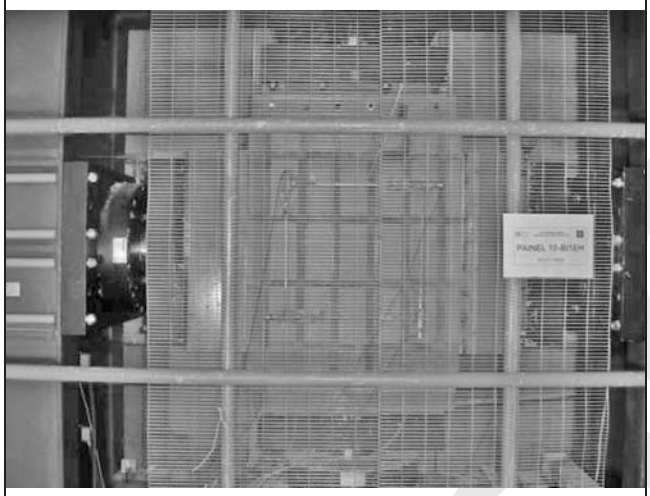

(b)

Fig. 3. Biaxial servo-controlled equipment: (a) view of the concrete side and (b) view of the masonry side

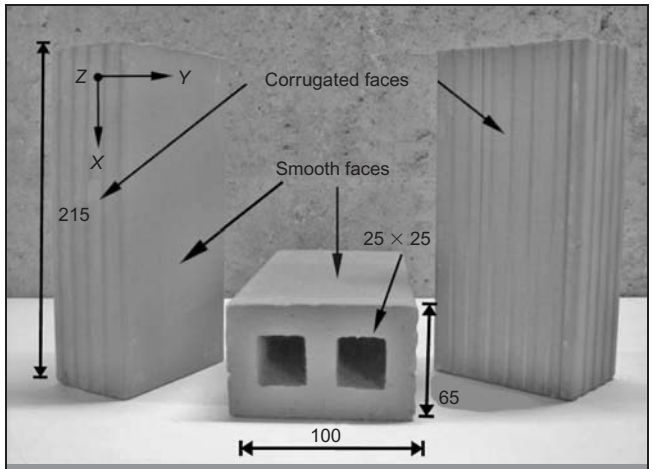

Fig. 4. Brick dimensions in mm

prototypes were submitted to four line loading configurations with a shear span length able to promote shear failure. The group of bending tests includes the series for assessing the influence of the orthotropy that results from the two possible arrangements of the brick elements and reinforcing bars.

To simulate the flexural behaviour of the reinforced masonry panels, a numerical model was applied, combining the moment–curvature relationship of each one of the distinct cross-sections of the panel and the matrix stiffness method.

To validate the developed structural system, a shell prototype was built and tested. The experimental research is described in the present paper, and the results are presented and analysed. The performance of the numerical model is appraised using the obtained experimental results. The effectiveness of the developed masonry shell structural system was assessed by building a real construction in the south of Italy. This topic is beyond the scope of the present paper, but a detailed description of this construction can be found elsewhere.[3]

2. EXPERIMENTAL PROGRAMME

2.1. Brick units

The geometric configuration of the brick units used in the developed shell structural system is shown in Fig. 4. The brick elements have the dimensions of 215 mm (length), 100 mm (width) and 65 mm (height), with holes of 25 mm × 25 mm, with three corrugated faces for better adhesion to the concrete and one smooth face (visible). The tensile and compressive strength and the Young's modulus of the bricks were obtained from tests. Tensile tests with specimens of a concrete joint bonded to one brick unit were also carried out, in order to evaluate the tensile bond strength.

2.1.1. Compression tests. The compressive strength in the X (longitudinal) and Y (transversal) direction for the brick units was 82 MPa and 32·8 MPa, respectively (average of eight dry specimens, with a CoV for the X and Y directions of 26% and 25%, respectively). The compressive strength was obtained according to EN 772–1.[4] The compression tests were displacement controlled at a rate of 1 μm/s. Fig. 5(a) shows a compression test performed in a brick unit loaded in the X direction.

2.1.2. Tensile tests. Tensile tests in bricks were displacement controlled at a rate of 0·05 μm/s. The four tested specimens had dimensions of 95·0 mm × 105·0 mm × 65·0 mm, height, width and thickness, respectively. Lateral notches of 3 mm of thickness and 2 mm of depth were opened at specimen mid-height to limit the crack propagation to the notched section. The displacements were registered by four external and one internal linear variable differential transducer (LVDT), see Fig. 5(b). An epoxy adhesive was used to fix the specimens to the load steel platens of the equipment and to ensure perfect alignment of the end plates.

The tensile strength, f_t, was calculated dividing the maximum load, F_u, by the area of the notched section. Typical relationships between the applied load and the average of the displacements recorded in the four external LVDTs are reproduced in Fig. 6. The typical large scatter of the tensile

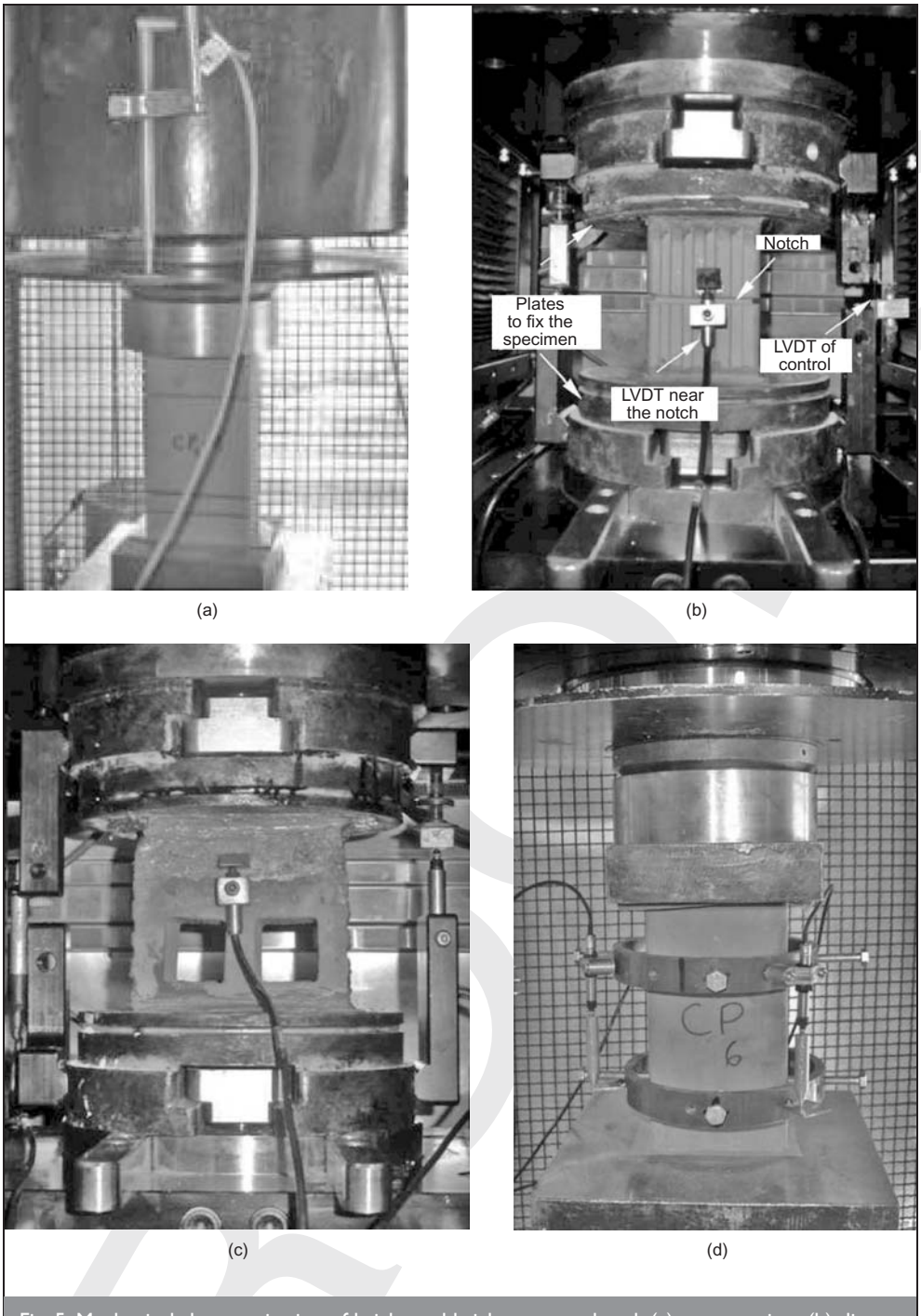

Fig. 5. Mechanical characterisation of bricks and brick-concrete bond: (a) compression, (b) direct tension, (c) brick–concrete bond test, (d) modulus of elasticity test

tests has been obtained, with an average strength value in the *X* direction of 0.91 MPa, with a CoV of 51.5%.

2.1.3. Brick–concrete bond. To assess the brick–concrete bond behaviour, uniaxial tensile tests were carried out according to the test set-up showed in Fig. 5(c). Fig. 7 represents the typical stress-displacement relationship for two distinct arrangements of the brick elements. The relationship of Fig. 7(a) corresponds to a specimen with the brick holes aligned with the applied load. This test arrangement intends to simulate the bond behaviour of the concrete joints in contact with the holes of the brick units, where a certain concrete volume penetrates into the brick holes. For this case, the bond strength is very high and an average value of 0.8 MPa was found. Fig. 7(b) corresponds to a brick with holes in the direction orthogonal to the applied load, which means that the concrete is bonded to the brick corrugated face. In this case the bond strength is much lower and an average value of 0.28 MPa was found.

2.1.4. Elastic modulus. The tests for the evaluation of the elastic modulus of the bricks were carried out according to the recommendation outlined in Ref. 5, see Fig. 5(d). The five tested bricks were submitted to five cycles of

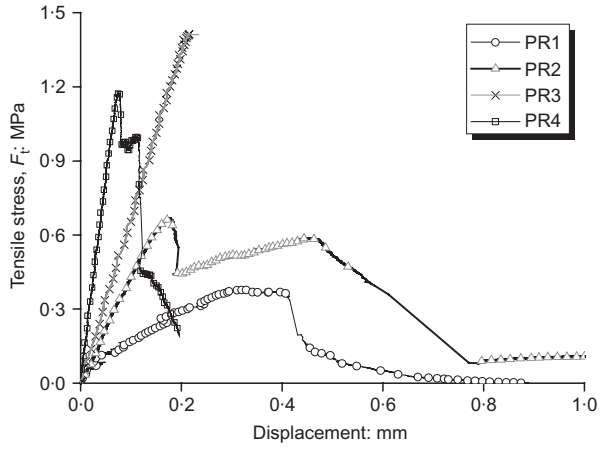

Fig. 6. Typical tensile stress-average displacement relationship in the direct tensile tests (four specimens are shown)

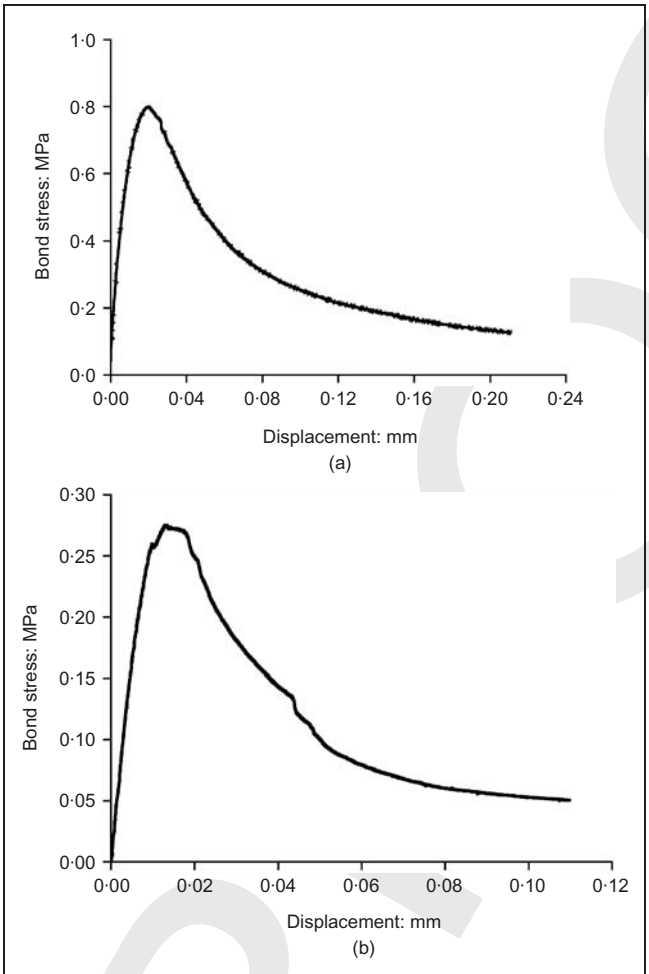

Fig. 7. Typical stress–displacement relationship in brick–concrete bond test with the brick holes in: (a) the direction of the applied load, (b) orthogonal direction to the applied load

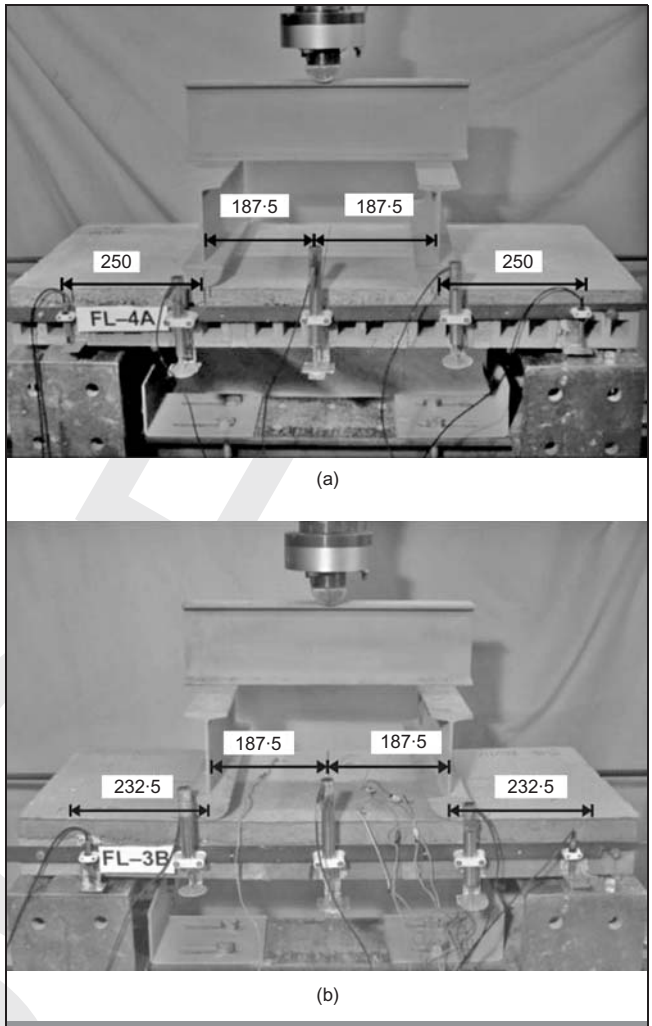

Fig. 8. Test set up for panels of series: (a) FL-A and (b) FL-B series

Materials		Be-1: kg/m^3	Be-2: kg/m^3
CEM I 42·5 R (C)		300	300
Fly ash (FA)		—	30
Sand	0·3–0·6 mm	279·32	273
	0·6–5 mm	654·70	710
Aggregate 5–10 mm		805·79	872
f_{cm}: MPa		38·23	22·61
		(2·87)	(1·21)
		[7·52]	[5·36]
$f_{ctm,fl}$: MPa		4·43	2·58
		(0·45)	(0·32)
		[10·19]	[12·57]
Superplasticiser 2·5% Rebuilt® 1000 (Be-2) and 1·5% Glenium ACE 32 (Be-3) water/fine ratio = 0·55			
Slump = 210 mm			

(value) Standard deviation
[value] CoV (%)

Table 1. Concrete composition per cubic metre and some concrete properties

compressive loading. The secant modulus was determined from the stress–strain relationship, where strains were evaluated from the displacements registered by the LVDTs. The angle between LVDTs was 120°. The average Young's

Bar diameter: mm	Tensile strength at 0·2%: MPa	Ultimate tensile strength: MPa	Young's modulus: GPa
3	545 (29·50) [5·41]	824 (56·31) [6·84]	200
6	668 (64·85) [9·71]	711 (73·05) [10·27]	217
8	524 (27·04) [5·16]	614 (17·46) [2·85]	195

(value) Standard deviation
[value] CoV (%)

Table 2. Main results obtained in the tensile tests of steel bars

Series	F_{cr}: kN	F_{sy}: kN	F_u: kN
FL-A	5·40	36·31	47·00
FL-B	13·61	36·00	53·32
FLI-A	12·72	23·19	28·48
FLI-B	22·31	29·83	30·18
FLC-1A	7·76	58·18	75·40
FLC-2A	7·70	60·42	73·17
FLC-1B	19·52	30·13	67·23
FLC-2B	22·96	33·32	82·17

Table 3. Main results of the tested series of panels

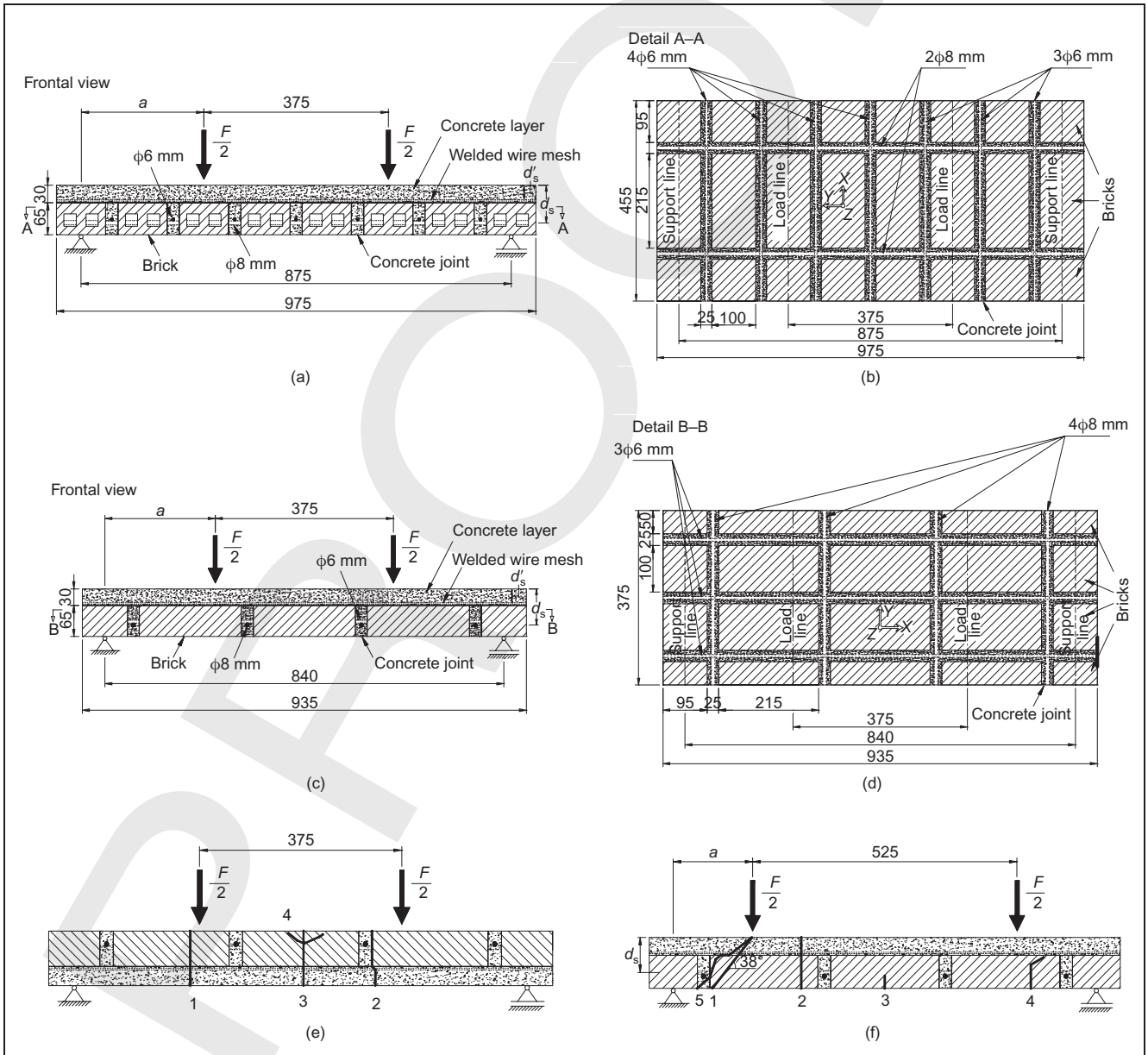

Fig. 9. Panels arrangements: (a) and (b) lateral and top view of panel A, series FL-A; (c) and (d) lateral and top view of panel B, series FL-B; (e) example of panel B tested with the concrete layer turned downwards; (f) frontal view of panel B tested with a shear span ratio, a/d, between 2·0 and 2·3 (FLC)

modulus found for the bricks was 21.42 GPa, with a coefficient of variation (CoV) of 20.7%.

2.2. Concrete

Table 1 presents the mix compositions used in the experimental programme, where f_{cm} is the mean value of compressive strength and $f_{ctm,fl}$ is the mean value of flexural tensile strength. The Be-2 mix exhibited better workability properties and finishing requirements for the shell prototype. It is necessary for the concrete's flowability to be sufficient to fill the joints and to assure good bond conditions with the reinforcement in the joints. Furthermore the viscosity level of the concrete must be enough to prevent concrete sliding out of the shell in the most inclined zones of the shell prototype.

Compression tests with cylinder specimens of 150 mm diameter and 300 mm height were carried out to assess the compression behaviour of the designed concrete. Three point bending tests with 850×150×150 mm^3 notched beams (a notch of 25 mm depth at beam mid-span) of 800 mm of span length were performed to obtain the concrete flexural behaviour. The tests were carried out according to Reunion Internationale des Lboratoires et Experts des Materiaux, Systemes de Construction et Ouvrges (RILEM) recommendations.[6,7]

2.3. Reinforcement

To assess the tensile behaviour of the ϕ8 mm and ϕ6 mm steel bars reinforcing the concrete joints orthogonal and parallel to the brick holes of the tested panels (see Fig. 2), tensile tests were performed according to recommendations given in Ref. 8. The wire mesh used to reinforce the concrete layer was made by ϕ3 mm bars forming a square grid of 75 mm spacing. Table 2 includes the main data obtained for all bars.

2.4. Tests with representative panels

2.4.1. Flexural behaviour of representative panels of reinforced masonry shells. Six series of four point bending tests on

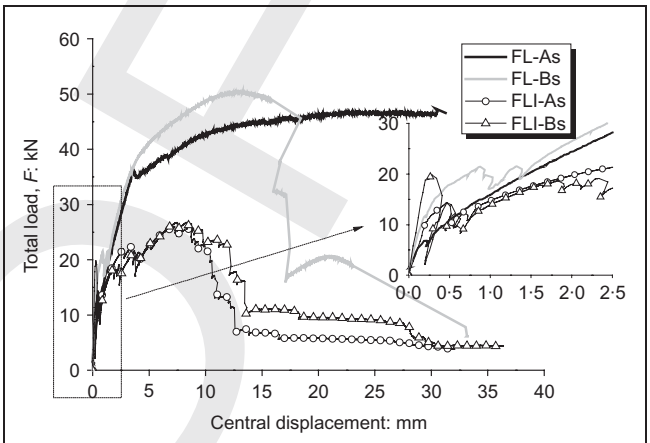

Fig.10. Average force–mid span deflection relationship of the series FL-A, FL-B, FLI-A and FLI-B

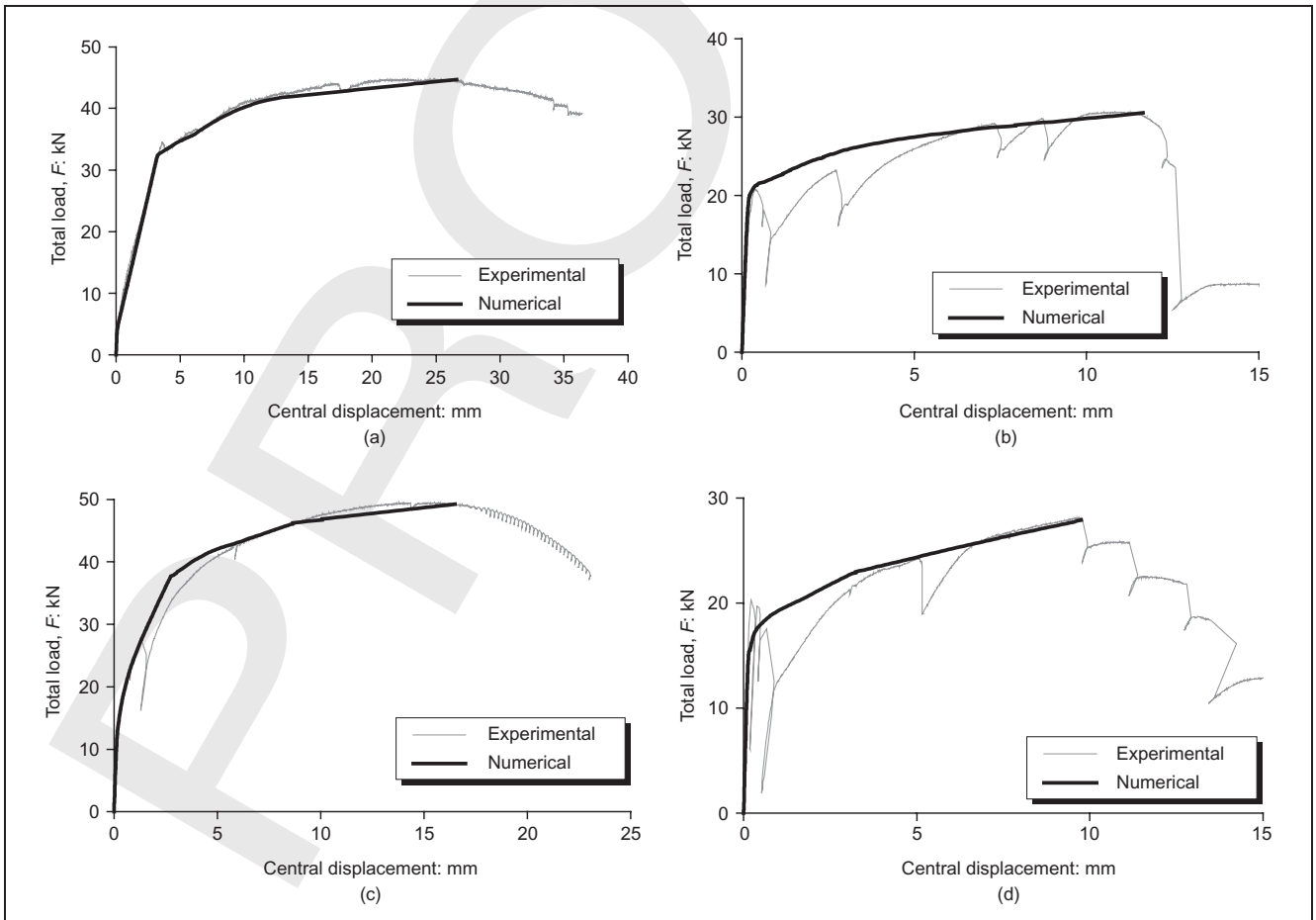

Fig. 11. Experimental plotted against numerical load–central deflection of panel: (a) FL-3A, (b) FLI-4A, (c) FL-3B and (d) FLI-3B

representative panels were carried out according to EN 1052–2,[9] see Fig. 8. The arrangements of the tested panels A and B are shown in Figs 2 and 9. To evaluate the behaviour of the structural system when submitted to positive and negative bending moments, a series of tests with the panel concrete layer turned upwards and downwards (Figs 2 and 9) was carried out. The influence of brick and reinforcement arrangements on the orthotropic behaviour of the structural element is analysed, comparing the behaviour of series FL-A and FL-B (see Figs 2(c) and 9). As this structure is not symmetric with respect to its mid-surface, its behaviour under positive and negative moments is distinct. Panels of a configuration equal to the FL-A and FL-B series were therefore tested with the concrete layer turned downwards. These series were designated by FLI-A and FLI-B, respectively. The shear resistance of the structural system was also evaluated by performing a test series FLC, with a shear span ratio, a/d, between 2.0 and 2.3 (Figs 2(i) and 9(f)). A total of 20 reinforced masonry panels were tested, grouped in four series of four panels (FL-A, FL-B, FLI-A and FLI-B) and two series of two panels (FLC-A and FLC-B). Series FL-A, FLI-A and FLC-A are further grouped as series FLA, while series FL-B, FLI-B and FLC-B are further grouped as FLB.

The bonding between brick and concrete joints, which is the weakest link of this system, had a marginal influence on the panel load-carrying capacity. Shear failure mode occurred only in one of the panels of FLC series.

Figure 10 shows the average load–central deflection of the panels. Table 3 includes the main results extracted from the tests (crack initiation load, F_{cr}, yield initiation load, F_{sy}, maximum load, F_u). Series FL-A and FL-B, with the concrete layer turned upwards, had a higher maximum load than series FLI-A and FLI-B, owing to the higher tensile longitudinal reinforcement ratio. The behaviour of the FLI-A and FLI-B series showed that the two analysed orthotropic arrangements of bricks and bars reinforcement have a marginal influence in terms of load-carrying capacity and stiffness. Despite the fact that series FL-B had a lower longitudinal reinforcement ratio than series FL-A ($A_s = 84.8$ mm^2 in FL-B and $A_s = 100.5$ mm^2 in series FL-A), series FL-B had a larger load-carrying capacity and stiffness than FL-A, which can be justified by the highest values of the yield and ultimate stress of the longitudinal ϕ6 mm steel bars used in the FL-B panels (see Table 2). The larger number of concrete ribs (joints) in the longitudinal direction of the FL-B panel series can justify the larger stiffness of these panel series (see Fig. 10). Moreover, in series FL-B, concrete of the transversal joints filled the ends of the brick holes, providing some interlock between bricks and concrete, while in the FL-A series concrete was bonded to the corrugated brick surfaces.

A numerical strategy was developed with the purpose of predicting the load–deflection relationship of the panels failing in bending. A cross-section layer model was used to determine the moment–curvature relationship, M–χ, of the representative sections of the tested panels, see Ref. 10. The M–χ was used to evaluate the tangential flexural stiffness, $(EI)_T$, of these sections during the panel loading process. The tangential stiffness matrix of the panel was evaluated from the $(EI)_T$ of each element discretising the panel, and using the framework of the matrix displacement method. The detailed description of the algorithm developed to simulate the deformational behaviour of structural elements failing in bending can be found elsewhere.[10] As Fig. 11 shows, this model reproduced accurately the load–deflection response observed in the tested panels.

2.4.2. Shear testing of stack bonded masonry. Shear tests in stack bonded masonry panels were carried out according to EN 1052–4.[11] Given the stacked nature of the masonry panels

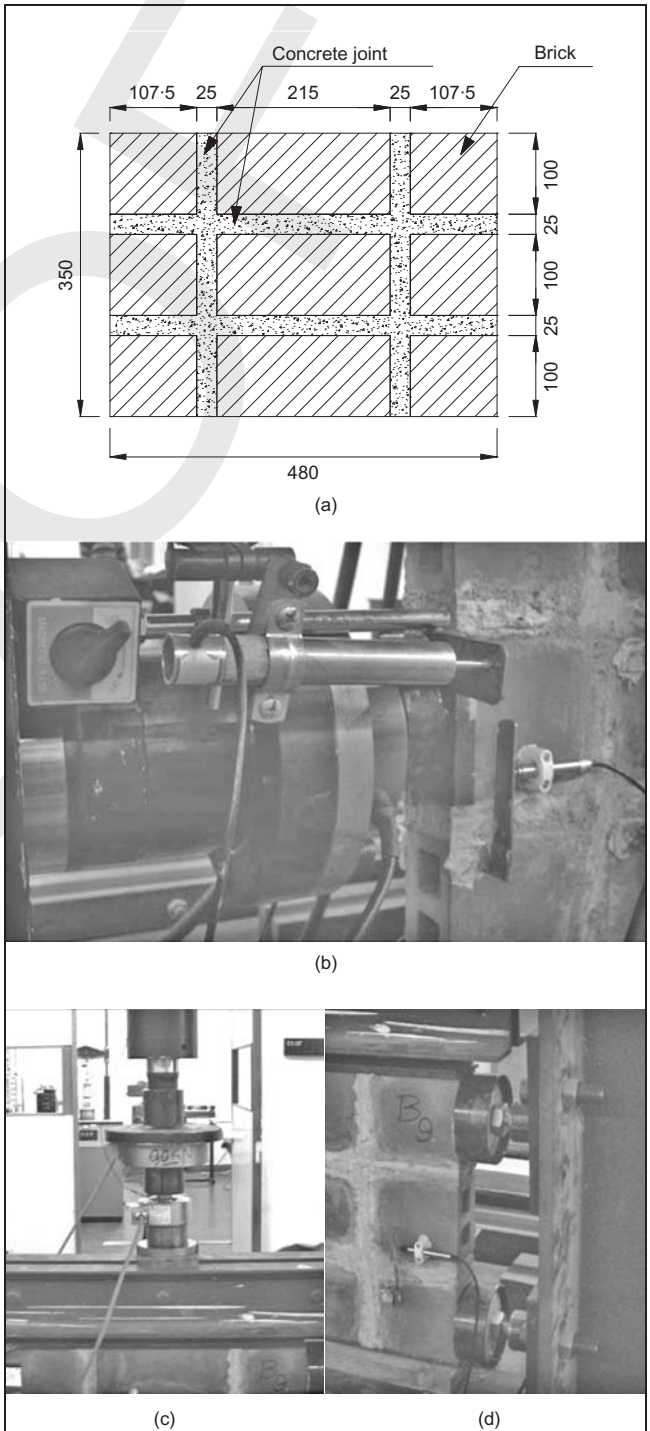

Fig. 12. Shear testing details: (a) specimen dimensions (mm); (b) actuator to apply shear force; (c) actuator of pre-compression load; (d) supports used to avoid horizontal displacement

and the novel use of micro-concrete Be-1 it was essential to use this standard instead of the triplet test detailed in EN 1052–3.[12]

In total, nine masonry specimens were tested, distributed in three series with three different normal pre-compression levels. The specimens consisted of three masonry courses subjected to a vertical pre-compression load, see Fig. 12. The specimen is kept under constant pressure while a horizontal load is applied in the middle masonry course by imposing increasing displacements with a hydraulic actuator of a maximum loading capacity of 250 kN. The horizontal load, measured with a load cell, was applied in order to assure a displacement rate of 20 μm/s of the movement of actuator's piston. This test set-up evaluates the shear strength of two joints simultaneously.

To define the cohesion and the friction angle of the joints, three different pre-compression stress levels were adopted: 0·2, 0·6 and 1·0 MPa. Fig. 13 presents typical failure modes of the tested panels, see Ref. 13 for details.

The displacements of the panel were registered by means of eight LVDTs. Four LVDTs were placed on the front of the specimens to measure the displacements in the horizontal direction, three LVDTs were placed on the back of the specimen to measure the vertical displacements and the last LVDT was used to control the test. Fig. 14(a) shows the relationship between the normal stress and the shear strength for all panels, as well as a linear regression carried out with the shear strength average for each series of tests. The correlation coefficient r^2 of the linear regression was 0.99, which indicates an excellent match. Fig. 14(b) presents typical relationships between the vertical and horizontal displacements, known as dilatancy. This parameter measures the uplift of one brick over the other upon shearing. It is known that dilatancy decreases to zero with the increasing of normal stress level.[14] Additionally, dilatancy decreases to zero owing to the smoothing of the sheared surfaces.

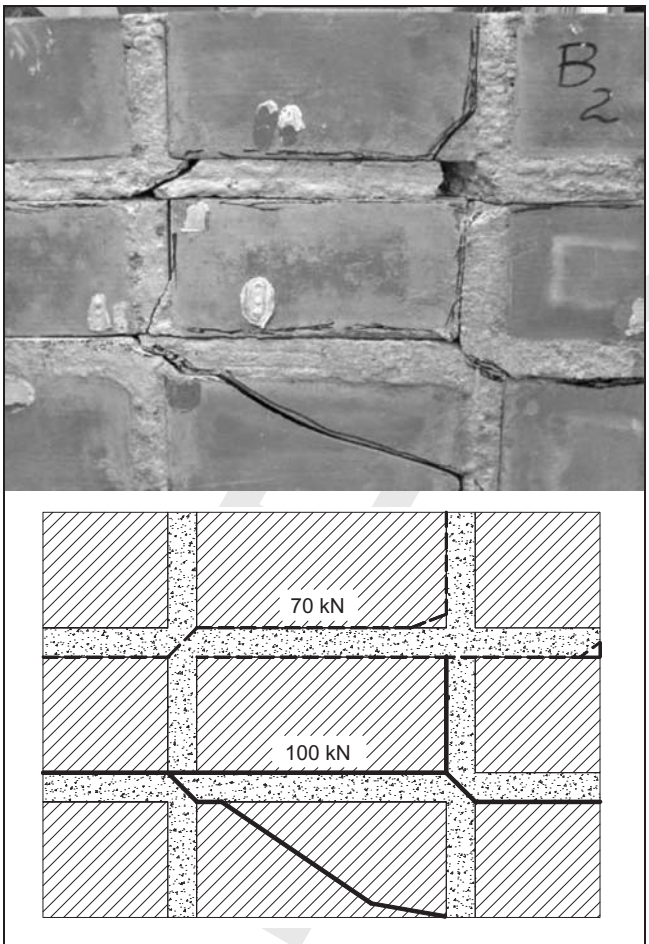

Fig. 13. Typical failure mode of the shear panels (Panel 2/pre-compression level 0·6 MPa)

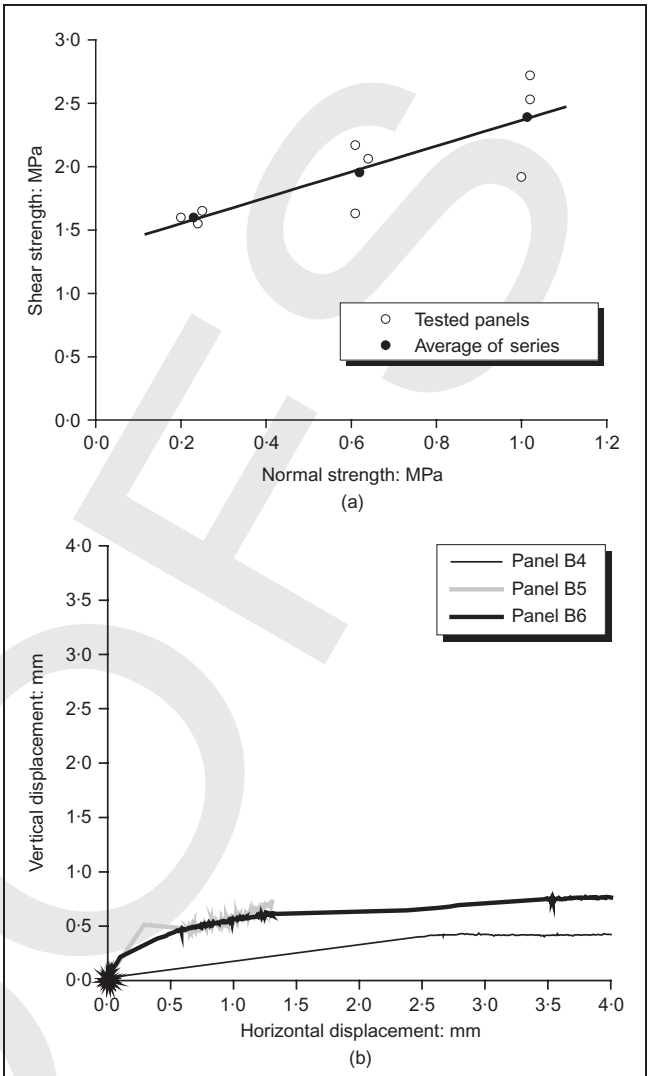

Fig. 14. Main results of shear tests: (a) shear strength for distinct normal stress levels, (b) typical relationship between horizontal and vertical displacements (pre-compression level of 0·6 MPa is shown)

The linear regression for the panels' strength provides a cohesion value c equal to 1·35 MPa and a tangent of the friction angle equal to 1·0. In standard masonry, the value of the tangent of friction angle seems to range between 0·7 and 1·2, according to different combinations of unit and mortar.[15] According to Ref. 11, the characteristic value of the initial shear strength or cohesion is only 80% of the experimental value, or 1.08 MPa in this case.

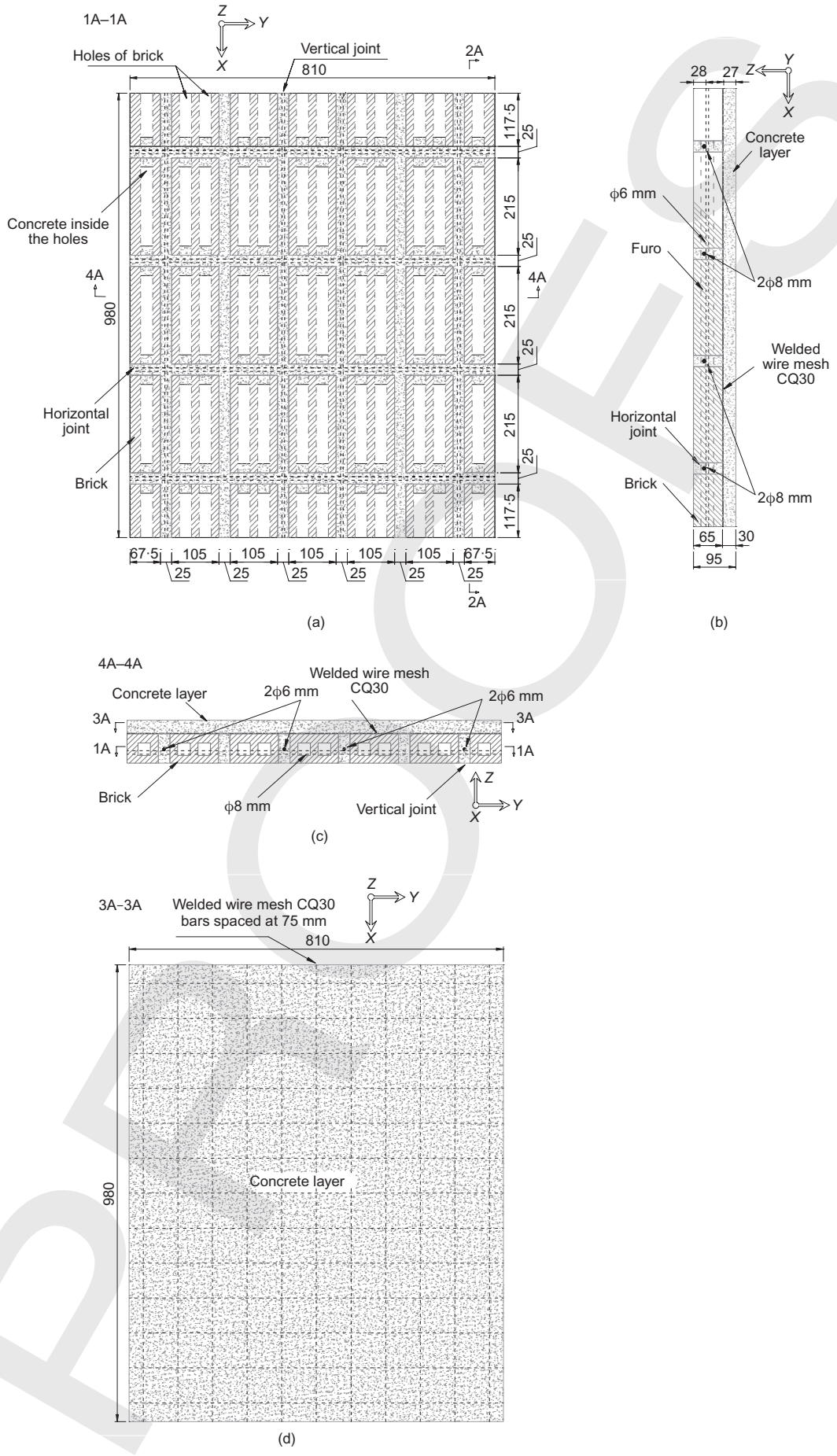

Fig. 15. Specimen configuration: (a) plan, (b) joints and steel bar positions, (c) vertical cross-section, (d) concrete layer and welded wire mesh

In conclusion, typical failure modes were obtained in the tests and the shear strength seems adequately to follow the Coulomb friction law. The use of a stacked configuration and the use of micro-concrete for the joints are therefore acceptable.

2.4.3. Biaxial tests. Biaxial compression tests involving panels of 810 mm × 980 mm × 95 mm, width, length and thickness, respectively, (see Fig. 15) were carried out. The reinforcement was made of steel bars of 8 mm and 6 mm diameter. The vertical reinforcement (ϕ6 mm) was placed in the two central and lateral concrete joints of the panel, in agreement with the shell reinforcement arrangement where transversal reinforcement was placed every two transversal joints and longitudinal reinforcement was placed in all longitudinal joints. In the concrete layer, immediately above the brick units, a welded wire mesh of bars of 3 mm diameter, spaced at 75 mm, was placed. The Be-1 micro-concrete (see Table 1) was used to infill both masonry joints and cover layer of 30 mm thickness. Transducer displacements (LVDTs) were placed in both sides of the panel: four in the concrete layer and four in brick layer, according to the arrangement shown in Fig. 16.

The horizontal and vertical loading axes were composed by an actuator of 2000 kN load capacity in compression and 200 kN in tension, and a fixed reaction system where the load cell was installed. The loading fixtures were composed by four steel platens that were mechanically connected to the actuators and to the fixed reaction systems. The steel platens connected to the actuator and to the reaction system of the vertical axis had a thickness of 150 mm, while steel platens of 200 mm thick were used for the horizontal axis. Two steel-teflon covered sheets with oil in between them were applied at the faces of the steel platens in contact with the faces of the tested panels in order to minimise friction, and, consequently, to assure, as much as possible, a uniform stress distribution in the zone of panel where the monitoring system was installed.

The panels were separated in groups taking into account the direction of the applied forces and the rate of displacement variation for each in-plane panel direction. The first load stage consisted of five cycles of incremental loading up to 490 kN, at a force rate of 2 kN/s. This load limit was chosen since it represents approximately 30% of the panel load-carrying capacity, if the panel is constituted by concrete only, and it was assumed that in this loading range the panel would have an elastic behaviour. In each cycle, after the target load has been attained it remained applied during a period of 30 s. After this loading cycle phase, the panel was submitted to monotonic loading under displacement control until panel failure, at a deformation rate of 0·005 mm/s, see Fig. 17. In biaxial compression, the tests were controlled by two displacement transducers, one for each direction. In uniaxial compression, under vertical and under horizontal loading configurations, the tests were controlled by the vertical and horizontal displacement transducers, respectively. Different ratios between the horizontal and vertical displacement were adopted according to the values indicated in Table 4. Here, the vertical, f_n, and horizontal, f_p, strength are obtained dividing the force by the panel cross-section in each direction.

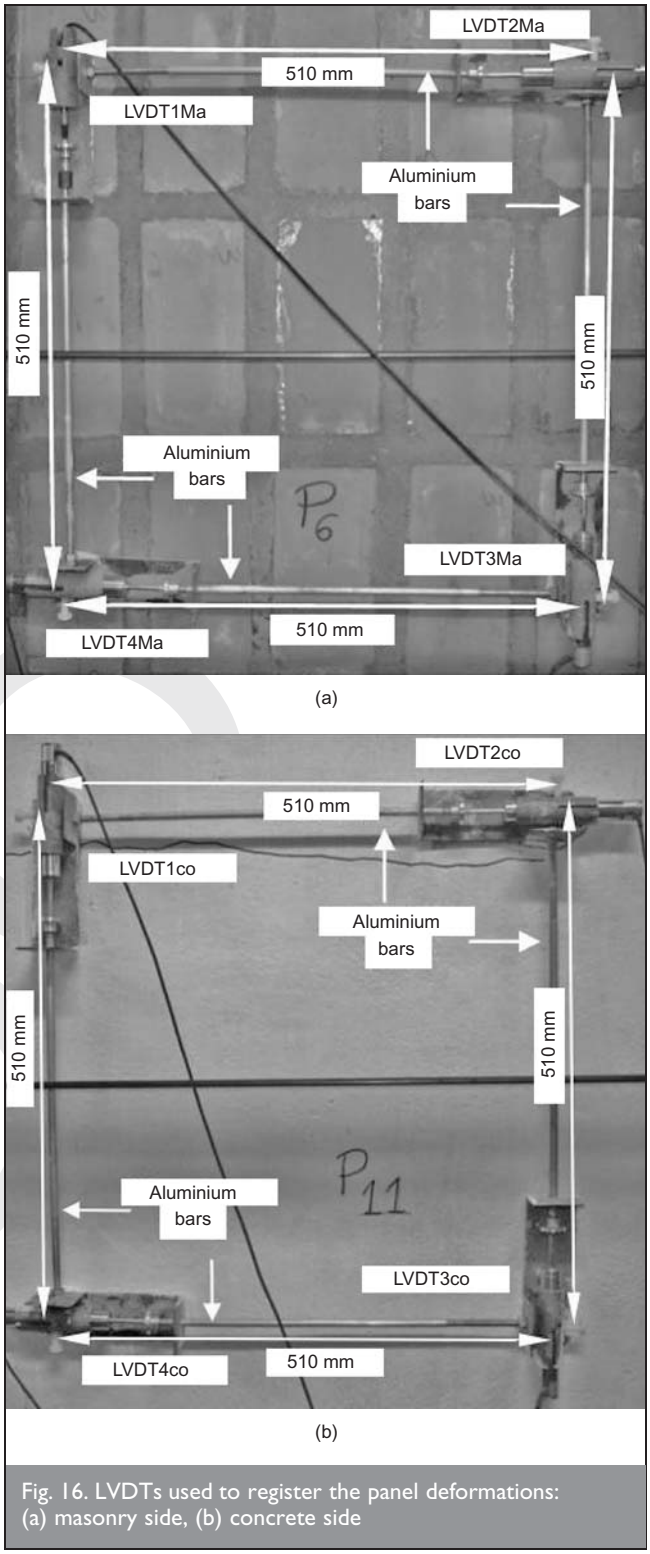

Fig. 16. LVDTs used to register the panel deformations: (a) masonry side, (b) concrete side

After GR1 group of tests have been carried out (the first one in this experimental programme), two changes were introduced in the test arrangement of the remaining test groups. The first change consisted of filling the holes of the bricks at the panel extremities with a grout of compressive strength 60 MPa at 28 days. The second change consisted of drilling the steel plates in the area in contact with the bars of the joints, in order to avoid buckling of the bars when the panel is loaded. These procedures made it possible to avoid the occurrence of local failures that could compromise the stability of the test and disturb the results. In fact, in the tests of the GR1 group, owing

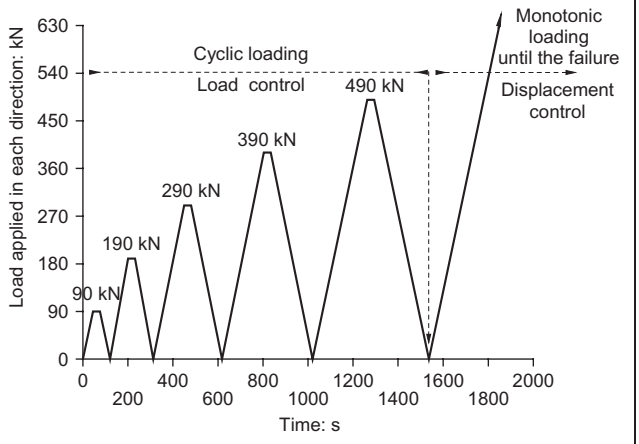

Fig. 17. Cyclic and monotonic loading procedures in the biaxial tests

to the buckling of steel bars in contact with the steel loading platens, concrete and parts of the bricks at the contour of the panel have spalled significantly.[16] From the obtained stress–deformation relationships[16] it was observed that filling the holes of the bricks in contact with the loading steel platens contributed to the increase in the stiffness of the panel, mainly in the horizontal direction. Furthermore, this procedure assured a better continuity between the distinct mobilised materials, which decreased the degree of anisotropy of the panel, leading to a better transference of the horizontal applied stresses to the central part of the panel. This was already reported by Hamid and Drysdale.[17]

The tests presented the following failure modes: crushing of the panel borders in contact with the equipment load platens; detachment of some brick walls; splitting at interface masonry/concrete layer; spalling through intermediate plane of the masonry layer. This failure mode was also observed by Dhanasekar *et al.*[18] and Naraine and Sinha.[19]

Figure 18 represents the curves relating the horizontal (σ_p) and vertical (σ_n) stresses recorded in the panels under biaxial tests. The $\sigma_p - \sigma_n$ curves are represented only up to the maximum horizontal stress, but the panels have supported vertical stresses larger than the values indicated in this figure. The curves of Fig. 18 show that the procedures adopted to avoid local failures at the contour of the panels have helped to assure a more regular distribution of stresses in the corresponding panels. For the panels P14, P16 and P18 f_n/f_p was about 0.5, while a value of around 1.3 was recorded for the panels P4, P6 and P19. In panels P5 and P15 f_n/f_p was about 1.7, while P17 and P20 presented values of 1.09 and 0.14, respectively.

Figure 19 presents the failure loads of all panels tested using the average values of f_n and f_p for each series of panel tests. The panels submitted to biaxial load have always failed owing to the collapse of the panel in its horizontal direction. The failure curves obtained by Page are also included in this figure.[20] Since the specimens of Page and those of the present experimental programme are significantly different in terms of the properties of the materials, presence or absence of reinforcement, arrangement of the brick elements and panel geometry, it is not possible to directly compare results. The behaviour of the representative panels of the reinforced

Groups	Panels	Direction of applied load	Displacement rate: mm/s		Stress: MPa	
			Horizontal direction	Vertical direction	Horizontal (f_p)	Vertical (f_n)
GR1	P4	Vertical and horizontal	5×10^{-3}	5×10^{-3}	12·23	16·86
	P5				9·57	16·71
	P6				11·66	14·70
GR2	P7	Vertical	—	5×10^{-3}	0	20·17
	P8				0	19·99
	P9				0	18·11
GR3	P10	Horizontal	5×10^{-3}	—	10·5	0
	P11				16·49	0
	P12				10·71	0
	P13				14·83	0
GR1R	P14	Vertical and horizontal	5×10^{-3}	5×10^{-3}	13·14	7·16
GR4	P15	Vertical and horizontal	5×10^{-3}	10×10^{-3}	9·73	16·2
	P16		10×10^{-3}	5×10^{-3}	11·38	5·21
	P17		5×10^{-3}	$7{\cdot}5 \times 10^{-3}$	14·39	15·64
	P18		$7{\cdot}5 \times 10^{-3}$	5×10^{-3}	10·73	5·36
	P19		3×10^{-3}	9×10^{-3}	9·9	12·28
	P20		9×10^{-3}	3×10^{-3}	10·85	1·56

Specimens P1–P3 were used to calibrate the testing system and the results of these specimens are not included in this table.

Table 4. Loading configuration in displacement control phase in the biaxial panel tests and vertical and horizontal stress at panel failure

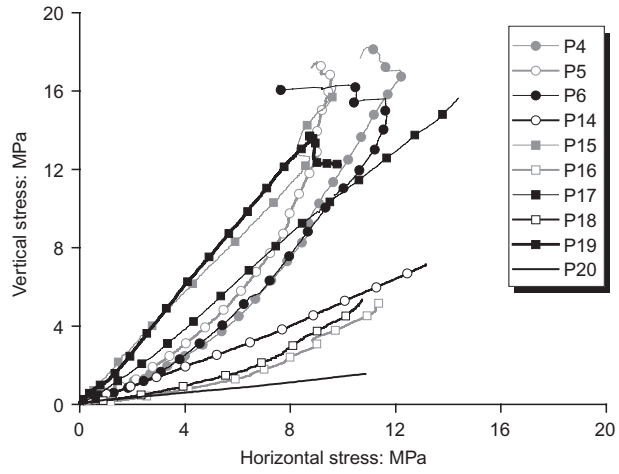

Fig. 18. Relationship between the vertical and horizontal stress in panels under biaxial tests

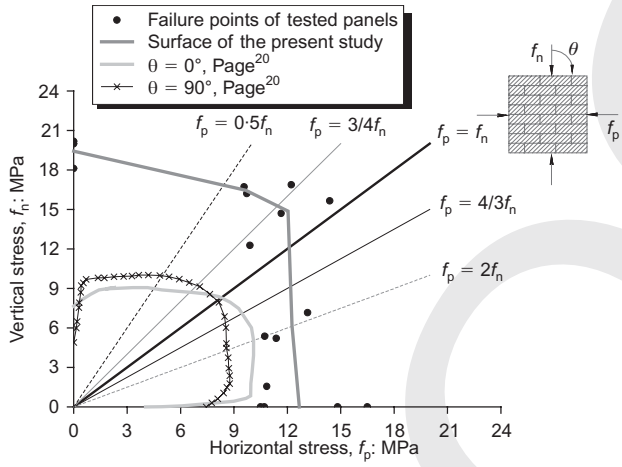

Fig. 19. Failure points on the f_p–f_n plane

masonry structural system is much more complex than the behaviour observed in panels of standard masonry.

2.5. Masonry shell

A reinforced masonry shell prototype was built at the Laboratory of the Structural Division of the Civil Engineering Department of University of Minho. The formwork of the shell had a catenary geometrical configuration with a span of 4 m and a rise of 1 m. The clay brick dimensions were 215 mm length, 100 mm width and 65 mm height. Polystyrene pieces were introduced in the extremities of the brick holes, to avoid excessive concrete penetration.

One steel bar of 8 mm diameter reinforced each longitudinal concrete joint, while one steel bar of 6 mm diameter reinforced each two transversal concrete joints. In the concrete layer, 10 mm above the brick units, a welded wire mesh of bars of 3 mm diameter, spaced at 75 mm, was placed.

The formwork was removed 24 h after the shell has been cast, to replicate a prefabrication scheme where the same formwork would be repeatedly used. Additional details on prefabrication can be found in Ref. 21. According to aesthetic requirements, concrete would not stain the exposed surface of the bricks, and concrete voids in the joints would not be acceptable. Fig. 20 reveals that these requirements were accomplished, meaning that the concrete consistency was appropriate for this application, both for the topping and for the joints.

The shell was tested under monotonic vertical load applied at a quarter of its span (see Fig. 21) and distributed along the shell width, using a HEB 200 steel profile for this purpose. The steel beam was supported on a wooden beam fixed with mortar to the top surface of the shell. The wooden beam geometry was chosen so that it would connect adequately the loading system to the shell curved geometry. The test was carried out under displacement control, using servo-controlled test equipment, at a displacement ratio of 15 μm/s. One of the six displacement transducers was fixed to the servo-hydraulic actuator of 100 kN maximum capacity in order to control the test from the displacement of the piston of the actuator. The load was measured by a load cell of 200 kN capacity, attached to the actuator. Three displacement transducers, LVDT 1–3 were positioned along the shell width under the line load, see Fig. 21. LVDT 5 was placed in mid span of the shell and LVDT 6 is at a symmetrical position of the line load

The shell was submitted to two monotonic loadings (c1 and c2). The c1 loading phase was interrupted when longitudinal reinforcement started yielding. The load in the shell was then removed. The second loading phase, c2, followed the same procedures than the first loading phase, c1.

Figure 22 shows, at about 15 kN, the significant decrease of the shell stiffness that occurred in the c1 loading phase owing to the occurrence of damages such as cracking of the concrete topping at the left part of the shell and cracking of the concrete joints under the line load, as well as debonding between concrete joints and bricks at the region of the line load. In the c2 loading phase, up to a load of

Fig. 20. Appearance of the shell bottom surface

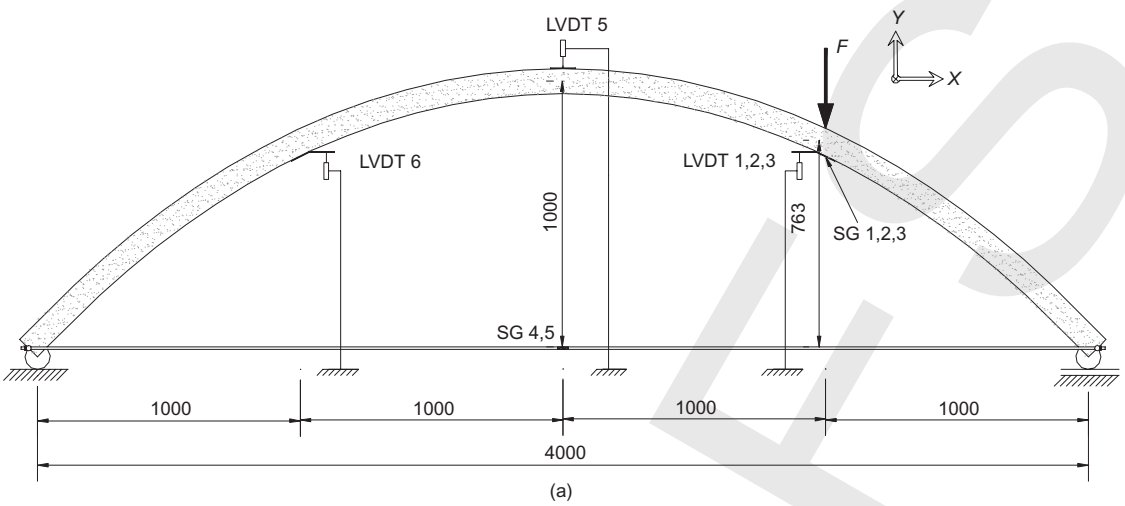

(a)

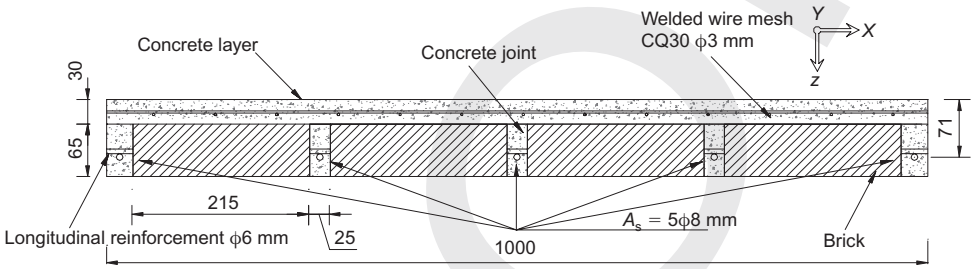

(b)

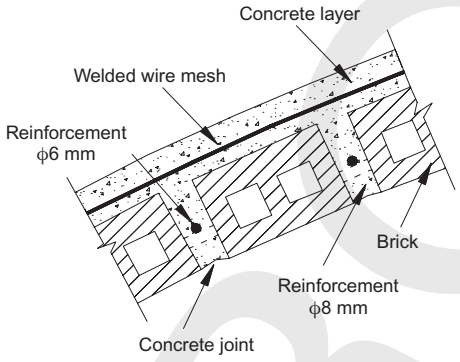

(c)

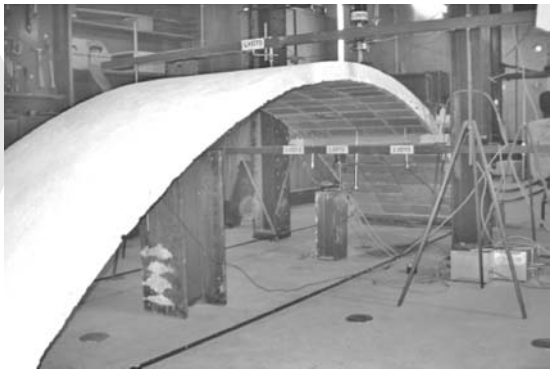

(d)

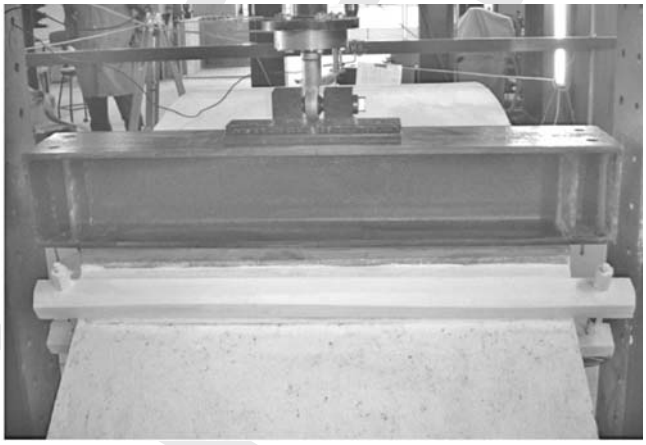

(e)

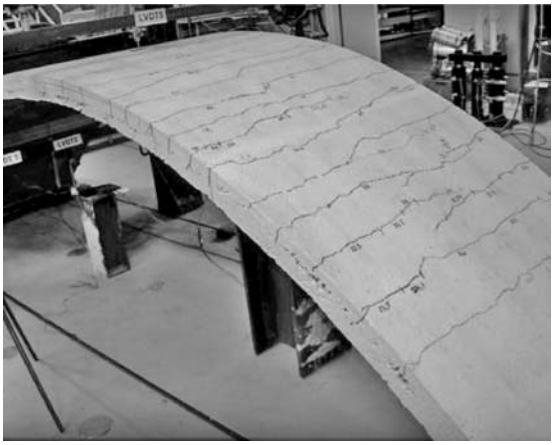

(f)

Fig. 21. Masonry shell: (a) shell geometry; loading configuration and instrumentation, (b) shell cross-section, (c) representative shell longitudinal section, (d) general view of the shell test set-up, (e) loading devices, (f) crack pattern

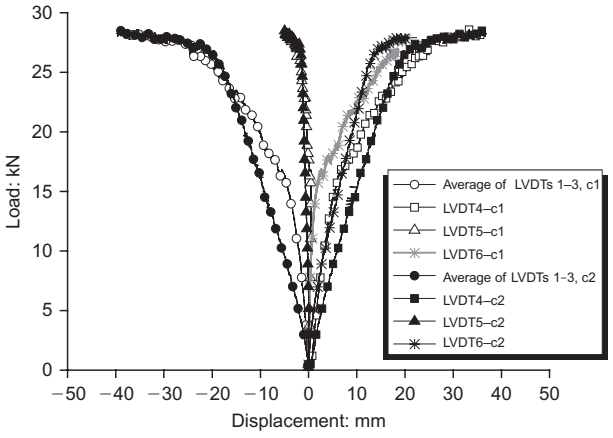

Fig. 22. Relationship between displacements registered by LVDTs and the applied load (c1—first loading and c2—second loading)

about 23 kN, since the shell behaviour does not have the contribution of the already cracked concrete and the already debonded concrete joints-bricks, the force-deflection at load line and the force–deflection at LVDT6 were not so stiff as in the c1 loading phase. After this load level, the responses of both loading phases were almost similar, however, and the ultimate load of 29 kN was reached for both loading phases.

To predict the load-carrying capacity of the developed shell, the equation that can be used to evaluate the bending moment at the line load section, $M_D(F)$, which is dependent on the load F (see Fig. 23(a)), was obtained assuming that materials have linear-elastic behaviour and the structure is statically indeterminate (one degree of redundancy). The positive resistant bending moment of the shell cross-section was obtained from the cross-section layer model already used in section 2.4. The moment–curvature relationship of the representative shell cross-section for positive moments is depicted in Fig. 23(b), from which a resistant bending moment of 12.1 kN/m was obtained. Replacing in the $M_D(F)$, the bending moment by this value, a maximum load of 28.6 kN was obtained, which is very similar to that registered experimentally, indicating that this simple approach can predict the load-carrying capacity of this type of structure.

3. CONCLUSIONS

The present article addresses the characterisation of reinforced masonry shells using a structural system including bricks, micro-concrete in a top layer and joints, and reinforcement in the joints and top layer. A comprehensive testing programme was established to characterise the constituents and masonry panels. Finally, a full-size masonry shell (span of 4·0 m) was cast and tested under point load at one-quarter span. This allowed the proposed solution to be validated from the technological and structural viewpoints.

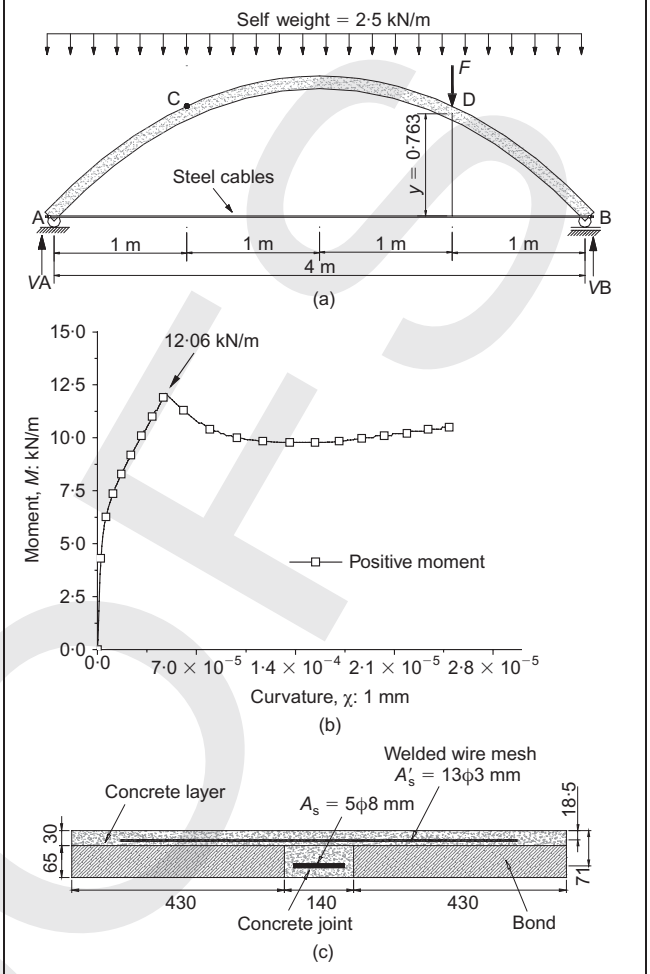

Fig. 23. Model for predicting the shell ultimate load: (a) shell loading, (b) moment–curvature relationship; (c) representative shell cross-section

ACKNOWLEDGEMENTS

This study is party sponsored by a research programme 'industrialized solutions for construction of masonry shell roofs' supported by the European Commission. Acknowledgements are also due to J. Monteiro & Filhos, SECIL, Bezerras's Quarry, and Bettor MBT Portugal. The first and third authors acknowledge the PhD grant provided by the Portuguese Science and Technology Foundation (FCT).

REFERENCES

1. DIESTE E. *Construire in Laterizio*, 1997, **52–53**, 156–179.
2. PEDRESCHI R. Eladio Dieste. *The Engineer's Contribution to Contemporary Architecture*. Thomas Telford, London, 2000, p. 160.
3. PIAGGIO *et al.* Analisi, prove e tecnologia costruttiva delle volte industrializzate in muratura armata (Analysis, tests and construction technology of reinforced masonry shell structures). *Construire in Laterizio*, 2005, **107**, 62–63 (in Italian).
4. COMITÉ EUROPÉEN DE NORMALISATION. *EN 772–1. Methods of test for masonry units. Part 1: determination of compressive strength*. CEN, Brussels, 2000, p. 14.
5. REUNION INTERNATIONALE DES LBORATOIRES ET EXPERTS DES MATERIAUX, SYSTEMES DE CONSTRUCTION ET OUVRGES (RILEM) TC14–CPC. Modulus of elasticity of concrete in compression. *Materials and Structures*, 1994a, **6**, No. 30, 25–27.

6. Reunion Internationale des Lboratoires et Experts des Materiaux, Systemes de Construction et Ouvrges (RILEM) TC14–CPC. Compression test on concrete. *Materials and Structures*, 1994b, **6**, No. 30, 17–18.
7. REUNION INTERNATIONALE DES LBORATOIRES ET EXPERTS DES MATERIAUX, SYSTEMES DE CONSTRUCTION ET OUVRGES (RILEM) TC 50–FMC. Determination of fracture energy of mortar and concrete by means of three-point bend tests on notched beams. *Materials and Structures*, 1994c, **18**, No. 106, 285–290.
8. COMITÉ EUROPÉEN DE NORMALISATION. *EN 10 002–1. Metallic materials – tensile testing. Part 1: method of test (at ambient temperature)*. CEN, Brussels, 1990. p. 35.
9. COMITÉ EUROPÉEN DE NORMALISATION. *EN 1052–2. Methods of test for masonry. Part 2: determination of flexural strength*. CEN, Brussels, 2000. p. 11.
10. BARROS J. A. O., OLIVEIRA J. T., BONALDO E. and LOURENÇO P. B. Flexural behavior of reinforced masonry panels. *ACI Journal,* 2006, **103**, No. 3, 418–426.
11. COMITÉ EUROPÉEN DE NORMALISATION. *EN 1052–4. Methods of test for masonry. Part 4: determination of shear strength including damp proof course*. CEN, Brussels, 2000, p. 16.
12. COMITÉ EUROPÉEN DE NORMALISATION. *EN 1052–3. Methods of test for masonry. Part 3: determination of initial shear strength*. CEN, Brussels, 2002. p. 18.
13. LOURENÇO P. B., BARROS J. O. and OLIVEIRA J. T. Shear testing of stack bonded masonry. *Construction and Building Materials*, 2004, **18**, 125–132.
14. LOURENÇO P. B. *Computacional Strategies for Masonry Structures*. PhD thesis, Delft University of Technology, 1996. p. 210.
15. PLUIJM R. V. D. *Out of Plane Bending of Masonry Behaviour and Strength*. PhD thesis, Eindhoven University of Technology, October, 1999. p. 259.
16. OLIVEIRA J. T. *Estudo Experimental Sobre a Pré-Fabricação de Cascas de Alvenaria Cerâmica Armada*. PhD thesis, University of Minho, 2005. p. 246.
17. HAMID A. A. and DRYSDALE R. G. Proposed failure criteria for concrete block masonry under biaxial stresses. *Journal of the Structural Division, ASCE*, 1981, **109**, ST8, 1675–1687.
18. DHANASEKAR M., PAGE A. W. and KLEEMAN P. W. The failure of brick masonry under biaxial stresses. *Proceedings of the Institution of Civil Engineers*, 1985, 295–313.
19. NARAINE K. and SINHA S. Cyclic behaviour of brick masonry under biaxial compression. *Journal of Structural Engineering,* 1991, **117**, No. 5, 1336–1355.
20. PAGE A. W. The biaxial compressive strength of brick masonry. *Proceedings of Institution of Civil Engineers*, London, 1981, 893–906.
21. SARRALBO V. Contribution to the viability of laminar reinforced masonry roofs using semi-prefabricated solutions. *Proposal for Short Span Cylindrical Shells*. PhD thesis, Universitat Politècnica de Catalunya, Barcelona, Spain, 2002 (in Spanish).